Mechanical Properties and Consequences of Stereocilia and Extracellular Links in Vestibular Hair Bundles

Jong-Hoon Nam,* John R. Cotton,* Ellengene H. Peterson,† and Wally Grant*

*Department of Engineering Science and Mechanics, School of Biomedical Engineering, Virginia Polytechnic Institute and State University, Blacksburg, Virginia 24061; and †Department of Biological Sciences and Neuroscience Program, Ohio University, Athens, Ohio 45701

ABSTRACT Although knowledge of the fine structure of vestibular hair bundles is increasing, the mechanical properties and functional significance of those structures remain unclear. In 2004, Bashtanov and colleagues reported the contribution of different extracellular links to bundle stiffness. We simulated Bashtanov's experimental protocol using a three-dimensional finite element bundle model with geometry measured from a typical striolar hair cell. Unlike any previous models, we separately consider two types of horizontal links: shaft links and upper lateral links. Our most important results are as follows. First, we identified the material properties required to match Bashtanov's experiment: stereocilia Young's modulus of 0.74 GPa, tip link assembly (gating spring) stiffness of 5300 pN/μm, and the combined stiffness of shaft links binding two adjacent stereocilia of 750 ~ 2250 pN/μm. Second, we conclude that upper lateral links are likely to have nonlinear mechanical properties: they have minimal stiffness during small bundle deformations but stiffen as the bundle deflects further. Third, we estimated the stiffness of the gating spring based on our realistic three-dimensional bundle model rather than a conventional model relying on the parallel arrangement assumption. Our predicted stiffness of the gating spring was greater than the previous estimation.

INTRODUCTION

Hair cells are the receptors of vertebrate inner ears. There are two broad groups; both detect mechanical stimuli. Auditory hair cells detect pressure waves in air or water to mediate hearing. Vestibular hair cells detect head movement; they are responsible for our sense of orientation in space and for reflexes that stabilize our gaze (1), posture (2,3), and vegetative functions (4).

Each hair cell is equipped with a mechanoreceptive organelle, the hair bundle, which comprises a hexagonal array of modified microvilli called stereocilia (5). The stereocilia are arranged in ''rows'' of increasing height, so that hair bundles can be said to have short and tall ends. Vestibular hair bundles also contain a true cilium at the tall end of the bundle, the kinocilium. Collectively, stereocilia and kinocilium form the ''hairs'' of the hair bundle. Mechanical stimuli bend these bundles. This alters the rate of transmitter release from hair cells onto postsynaptic neurons called primary afferents, which causes them to modify their firing. The modification of afferent firing is the signal that the inner ear transmits to the central nervous system.

Stereocilia and kinocilium are interconnected by extracellular, filamentous structures called links. Five types of links have been described in vestibular hair cells, based on their location in the hair bundle (for a review, see Bashtanov et al. (6)): 1), kinocilial links (KLs) connect the kinocilium to one or more of the tallest stereocilia; 2), ankle links and 3), shaft links (SLs) interconnect the tapered bases and cylindrical shafts, respectively, of adjacent stereocilia; 4), upper lateral links (ULs) run horizontally, interconnecting the stereocilia near their tips; and 5), tip links run obliquely from the tip of a shorter stereocilium up to the shaft of the next taller stereocilium. Considerable evidence suggests that the five link types differ in structure and chemical composition (7–17). Thus, they are likely to differ in mechanical properties.

It would be useful to know the mechanical properties of bundle constituents (stereocilia, kinocilium, and different link types) because this would help us understand the role each plays in mechanoreception by hair bundles. Because bundle constituents are very small and delicate, it is difficult to measure their mechanical properties experimentally. Models provide an alternative approach, but few previous models have addressed the mechanical properties of individual bundle constituents. They have incorporated the effects of all constituents except tip links into a single ''pivot spring'' (18–21) or lumped shaft connectors and ULs together as ''lateral links'' (22–28). The latter approach produced a dilemma: if these lateral links are compliant, they cannot prevent splaying of the bundle, but stiff lateral links prevent stimulus energy from being transmitted effectively to transduction channels. To solve this dilemma and uncover the role of different bundle constituents, we need to investigate the contribution of bundle constituents individually. Recent advances in our understanding of link structure and increasingly sophisticated computational models together enable us to address this need.

In this study, we used finite element (FE) modeling to investigate the mechanical properties of stereocilia and different link types. FE analysis is an established tool for analysis of structural, thermal, and electromagnetic problems. An advantage of the FE method is its ability to model complicated geometries such as the varied and complex shapes of hair bundles. The flexibility and generality of FE analysis for

Submitted May 9, 2005, and accepted for publication December 5, 2005.

Address reprint requests to John R. Cotton, Norris Hall, Blacksburg, VA 24061. Tel.: 1-540-231-7979; E-mail: jcotton@vt.edu.

0006-3495/06/04/2786/10 $2.00

doi: 10.1529/biophysj.105.066027

investigating hair bundle mechanics was shown in previous studies (24–29). Our FE models incorporate important features of in vivo bundles including 1), realistic, three-dimensional (3-D) structure; and 2), new experimental findings on the composition of some link types.

We took advantage of a recent study which measured the stiffness of chick vestibular hair bundles before and after removal of different link types (6). By using our FE model to simulate these experiments, we determined the mechanical properties of stereocilia, tip links, ULs, and SLs that fully explain the experimental results of Bashtanov et al. (6). Our results also provide insights into the functional role of different link types.

METHODS

Finite element program

For this analysis we have used a custom-made FE program and algorithm originally presented in Cotton and Grant (25). The previous FORTRAN program was newly written and run in MATLAB (The MathWorks, Natick, MA). The hair bundle FE model is composed of two types of elements. The stereocilia are represented by Timoshenko (shear deformable) beam elements (30), which describe well the anisotropy of the stereocilia and account for translation and rotation under shear and moment loads. For the tip links, ULs, SLs, and KLs an elastic rod element is used which can either elongate or shrink. These links can support no bending or shear forces. Ankle links are neglected in the model as they contribute little structurally (6). The element mesh size for the stereocilia ranged from 0.05 to 1.0 μm after considering the real geometry of hair bundle, the matrix condition number, and the computational efficiency. It was confirmed that the solution with a refined mesh yields no difference. The custom program was validated by solving a simple problem and comparing it with the solution from a commercial FE program.

Modeling the vestibular hair bundle

The experiments of Bashtanov et al. (6) used bundles from the utricular striola. The utricle is a subdivision of the vestibular labyrinth that detects linear head acceleration in the horizontal plane and head tilt; the striola is a band of specialized utricular hair bundles. Bashtanov et al. used striolar bundles from chicks. Unfortunately, not enough quantitative information is available on the structure of chick bundles to use them in our FE models. Accordingly, we modeled one hair bundle type from the utricular striola of a turtle, *Trachemys* (*Pseudemys*) *scripta*, in part because this bundle type resembles chick utricular bundles qualitatively and in part because we have detailed quantitative information about its structure (31,32). This bundle type forms a 20-μm-wide band within the striola (zone 2, (31)) just medial to the line of polarity reversal (LPR; the tall ends of utricular bundles face each other across this reversal line).

Model construction procedures are illustrated in Fig. 1. Information on the planar arrangement of stereocilia was obtained from confocal micrographs taken at the base of utricular hair bundles viewed in whole mounts (Fig. 1 *a*). Heights of stereocilia and kinocilium were taken from confocal micrographs showing bundles in lateral view (Fig. 1 *b*). Because it is impossible to measure both planar arrangement of stereocilia and bundle heights from the same cell, heights of stereocilia and kinocilium were inferred from the average values of hair cells at the same location (zone 2, (32)). These geometric properties are presented in Table 1.

The configurations of interciliary link structures followed previous studies (7–10,12–17,33,34). Link configurations for vestibular bundles have been summarized by Goodyear and Richardson (8) and Bashtanov et al. (6)

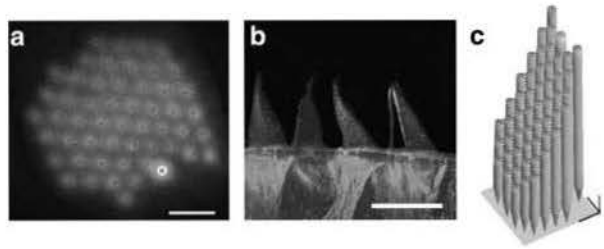

FIGURE 1 Constructing the 3-D FE model. (*a*) Number, arrangement, and spacing of stereocilia are obtained from the planar view at the base of a hair bundle. This confocal micrograph shows labeled stereocilia (*bright circular profiles*) from a turtle striolar hair bundle. Superimposed on them (*dots*) is the stereociliary array used in our model. K: kinocilium. (*b*) The heights of the kinocilium and the tallest and shortest stereocilia are measured from side views of bundles from the same macular location. The resultant FE model of a striolar hair bundle from the turtle utricle is shown in panel *c*. The scale bar in the right bottom corner indicates 1 μm in panels *a* and *c* and 10 μm in panel *b*.

and duplicated in our FE model (Fig. 2 *a*). In the FE model, the spatial densities of the horizontal links (ULs, SLs, and KLs) are lower than occur in vivo. There are two reasons for this. First, little or no quantitative information is available about the position and spacing of horizontal links. Second, we could achieve the same mechanical effect and greatly reduce run times by modeling links at a lower density. Therefore, we chose 0.2 μm for the spacing of ULs and the KLs and 0.5 ~ 1.0 μm for the spacing of SLs. As a result, the proposed mechanical properties of these links do not represent the mechanical properties of single filaments. Instead, the stiffness of each model link represents the collective mechanical effect of multiple filaments. The effect of the different spacing in the model and in real hair cell bundles is discussed later.

The tip links in the FE model represent all the structural components connecting the core cytoskeletal structure of one stereocilium to the core of the other stereocilium. Those structural components include the extracellular helical segment, probably composed of Cdh23, the transduction channel(s) with their associated elastic elements, Myo1c molecules, and other unknown intracellular and extracellular proteins (35–38). To avoid confusion with the

TABLE 1 Geometric properties of the model

Region	Striola
No. of stereocilia	51 (+1 kinocilium)
Height of kinocilium	8.8 μm
Tallest stereocilia	9.2 μm
Shortest stereocilia	2.4 μm
Stereocilia spacing	0.48 ± 0.026 μm
Diameter of kinocilium	0.425 μm
Diameter of stereocilia (shaft/root)*	0.4/0.04 μm
Lateral link length (mean ± SD)*	0.078 ± 0.026 μm
Tip link length (mean ± SD)*	0.227 ± 0.003 μm
No. of tip links	42
No. of UL between two stereocilia	3 or less
No. of SL between two stereocilia	3 or less
Array length in E-I direction	3.18 μm
Bundle height slope†	2.14
Width/length‡	1.01

*These values were not measured; the stereocilia shaft diameters were adjusted to have the tip link length of ~220 nm.
†Height difference between the tallest and the shortest stereocilia divided by the array length in E-I direction. A linear height gradient is assumed.
‡Array width perpendicular to the hair cell E-I direction divided by the array length.

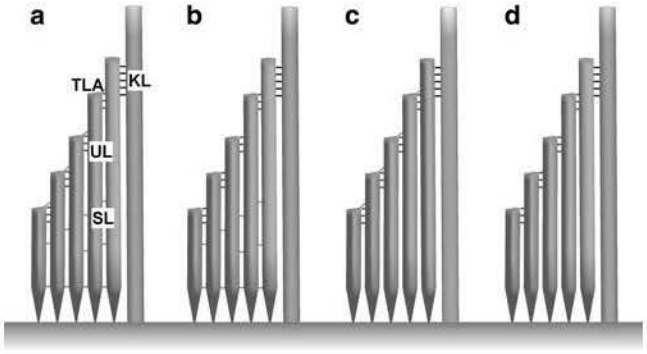

FIGURE 2 Two-dimensional images depicting the links between stereocilia. Only the central column that includes the kinocilium is drawn to show the different links in the hair bundle FE models. (*a*) Control hair bundle: the studied striolar hair bundle has TLA, UL, SLs, and KLs. Three cases were tested to observe the contribution of each structural component to the overall bundle stiffness. The cases include (*b*) hair bundle without tip links, (*c*) hair bundle without SLs, and (*d*) hair bundle without tip and SLs. These three cases reproduce the experimental conditions of Bashtanov et al. (6).

tip links recognized by electronmicroscopy, we will refer to this transduction complex as a tip link assembly (TLA).

Simulation protocol

We simulated the experiment of Bashtanov et al. (6). Like the experiment, four cases were run to determine the structural contribution of different link types and to estimate the mechanical properties of the bundle structural components (Fig. 2, *a–d*). Link structures of a hair bundle include the TLAs, the ULs, the KLs, and the SLs. In addition to these links, the flexibility of stereocilia roots affects the bundle compliance.

To measure the stiffness of the hair bundle in a resting state, a small point load of 1.0 pN in the excitatory direction (toward the taller edge) is applied at the tip of the kinocilium. The deflection at the tip of the kinocilium is computed and the bundle stiffness is defined as the applied load divided by the tip deflection. The hair bundle without tip links (Fig. 2 *b*) represents the BAPTA treated hair bundle. The hair bundle missing SLs (Fig. 2 *c*) represents the subtilisin treated hair bundle. A hair bundle washed with BAPTA and subtilisin has no tip or SLs (Fig. 2 *d*).

Throughout the study, we varied only four mechanical parameters: the stereocilia Young's modulus (E_S), the stiffness of the TLA (k_{TLA}), the ULs (k_{UL}), and the SLs (k_{SL}). We began by identifying a set of optimal mechanical parameters (E_S*, k_{TLA}*, k_{UL}*, and k_{SL}*) that minimize the difference between the modeled results and the three experimental outcomes of Bashtanov et al., namely 43% and 48% stiffness reduction after tip and SL removal and the intact bundle stiffness of 900 pN/μm. Initial values of E_S, k_{TLA}, k_{UL}, and k_{SL} were taken from the previous study (28). We then held three of the parameters constant and found the value of the fourth that minimized the difference. We repeated this process for the other three parameters in turn and then repeated the entire process until the values converged.

After we identified the optimal mechanical properties (E_S*, k_{TLA}*, k_{UL}*, and k_{SL}*), we performed a series of parametric studies to observe the effects of each individual mechanical parameter on the whole bundle stiffness. In each of four parametric studies, three of the optimal mechanical properties were fixed and the remaining parameter varied.

Fixed mechanical parameters

During estimation of the parameter values described above, we fixed four additional parameter values: 1), the stiffness of KLs (10^4 pN/μm), 2), the Young's modulus (0.13 GPa) and 3), the shear modulus (0.045 GPa) of the kinocilium, and 4), the shear modulus of stereocilia (0.74 MPa). This study also consistently assumed the mechanical boundary conditions of fixed stereocilia roots and hinged kinocilium root.

KLs connect the kinocilium with the rest of the bundle. They have much in common with extracellular tip links (10,16), and these extracellular tip links are considered inelastic and very stiff (12,15). We rationalize that the KLs should also be stiff as these links function merely to couple the forced kinocilium to the rest of the bundle structure, and compliance would serve no purpose. Our model showed that, as long as the KL stiffness is greater than a few thousand piconewtons/micrometers, bundle compliance is not affected by the KL stiffness. The kinocilium mechanical properties were inferred from those of sperm flagella and assumed to be isotropic (39). The shear modulus of stereocilia is set to 1/1000 of the Young's modulus based on results of previous parametric studies (26,29,40). In this study, we observed that a stereocilia shear modulus has a minor effect on the overall bundle stiffness or the stiffness contribution by different structural components. A stereocilia shear modulus even a hundred times greater than the value used for the study changed the bundle stiffness only a few percent and the relative stiffness contribution by <1%.

The mechanical boundary conditions are important and can affect the bundle stiffness considerably. Because the cuticular plate on which the stereocilia stand is a dense tangle of actin fibers into which the stereocilia fibers in the root completely embed (41,42), a clamped boundary condition was applied in which stereocilia cannot translate or pivot at the insertion point (29). The surface on which the kinocilium stands is considered much more compliant than the cuticular plate (43). For the kinocilium, a pinned boundary condition is applied in which the root of the kinocilium cannot translate but can freely pivot. In an early model with a clamped kinocilium root (data not shown), the stiffness contribution of the kinocilium was so large that the removal of tip or SLs could never reduce the bundle stiffness more than 30%, which is inconsistent with experimental results.

RESULTS

Mechanical properties of hair bundle structural elements

The mechanical properties satisfying Bashtanov's et al. results were identified: Young's modulus of stereocilia, 0.74 GPa, and stiffness of TLA and ULs and SLs of 5300, 1, and 750 pN/μm, respectively. These values matched the solution obtained from the simplex method. In Table 2, the hair bundle stiffness and contribution of each structural element with the identified mechanical properties are compared with the experimental results (6). With the identified mechanical properties, our computational model produced the same results as the experiment. How the identified mechanical properties match other studies will be described in the discussion.

Parametric study

We used parametric analyses to learn the effects of each mechanical parameter on total bundle stiffness with all links

TABLE 2 Hair bundle stiffness with identified mechanical properties

Case	a (Stiffness pN/μm)	b (Stiffness reduction %)	c (Stiffness reduction %)	d (Stiffness reduction %)
Bashtanov et al. (6)	900 ± 500	43 ± 18	48 ± 14	N/A
This study	901	43.5	48.3	80.8

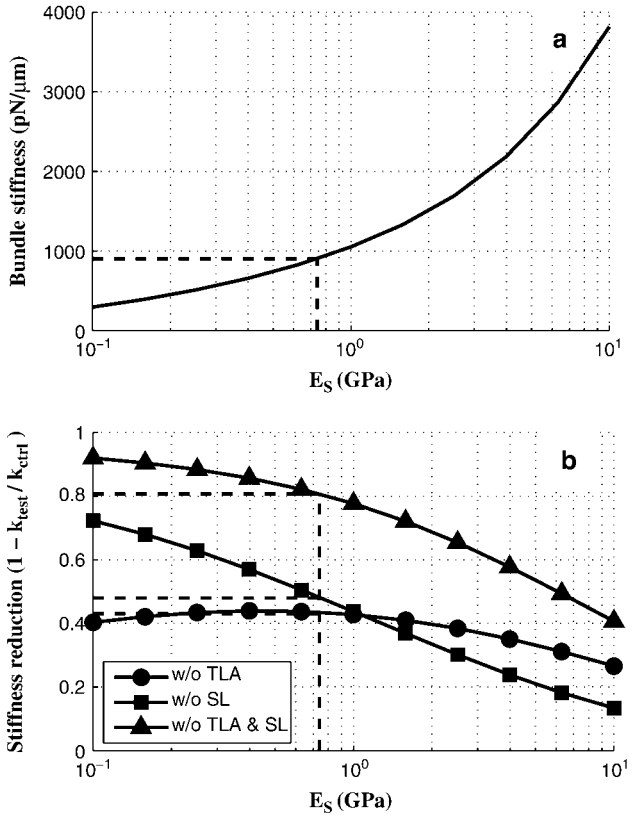

FIGURE 3 Effect of stereocilia Young's modulus (E_S) on the hair bundle stiffness. At $E_S = 0.74$ GPa, the bundle stiffness matched the experiment results (*dashed lines*). (*a*) Bundle stiffness versus stereocilia E_s: the bundle stiffness increased from 300 to 3820 pN/μm as the E_s increased from 0.1 to 10 GPa. (*b*) Structural contribution of different links: as the E_S increased, the $\bar{k}_{SA}$ decreased, but the $\bar{k}_{TL}$ stayed at a similar level when E_S was 0.3 ~ 1.2 GPa.

intact (panels *a* in Figs. 3–6) or after one or more links were severed (panels *b* in Figs. 3–6). In these figures the value that we estimated for each mechanical property (see Mechanical properties of hair bundle structural elements, above) is marked by a vertical dashed line. Horizontal dashed lines mark values for total bundle stiffness (panel *a* of each figure) or stiffness reduction (panel *b*) reported by Bashtanov et al. and matched in this study.

The stiffness of the striolar hair bundle was tested for different stereocilia Young's modulus values (Fig. 3). As the Young's modulus was increased from 0.1 to 10 GPa, the bundle stiffness increased from 300 to 3820 pN/μm (Fig. 3 *a*). We defined the stiffness contribution or the fractional stiffness reduction of the TLAs as $\bar{k}_{TL} = (k_0 - k_{w/oTL})/k_0$, where k_0 is the stiffness of the control hair bundle and $k_{w/oTL}$ is the stiffness of the hair bundle after removing the tip links. Likewise $\bar{k}_{SL}$ and $\bar{k}_{UL}$ denote the fractional stiffness reductions after the SLs and the ULs are removed, respectively. Finally, $\bar{k}_{SLTL}$ is the fractional stiffness reduction after both the shafts and the tip links are removed. The contribution of each structural element can be inferred from the stiffness reduction after removing that element (Fig. 3 *b*).

The structural contribution by the SLs decreased as the stereocilia got stiffer (Fig. 3 *b*). The SL contribution $\bar{k}_{SL}$ went from 0.72 for lower stereocilia modulus to 0.13 for higher stereocilia modulus. On the contrary, the TLA contribution, $\bar{k}_{TL}$, did not vary monotonically and was not affected much by stereocilia Young's modulus. As the Young's modulus of stereocilia changed from 0.5 to 1.0 GPa, the $\bar{k}_{TL}$ stayed between 0.42 and 0.44.

Varying TLA stiffness also affected the whole bundle stiffness (Fig. 4). As the stiffness of TLA was increased a hundred times from 100 to 10,000 pN/μm, the bundle stiffness doubled from 530 to 1000 pN/μm (Fig. 4 *a*). Because the SLs and the TLAs both can play the role of binding the bundle, as the stiffness of TLA was increased, the contribution of TLAs $\bar{k}_{TL}$ increased from 0.04 to 0.49, whereas the contribution of the SLs $\bar{k}_{SL}$ decreased from 0.61 to 0.48. Experimental studies show that the stiffness of a hair bundle is decreased after removing the tip links (44,45). According to our simulated result, for the TLAs to contribute more than 30% of bundle stiffness, the TLA should have stiffness >1600 pN/μm.

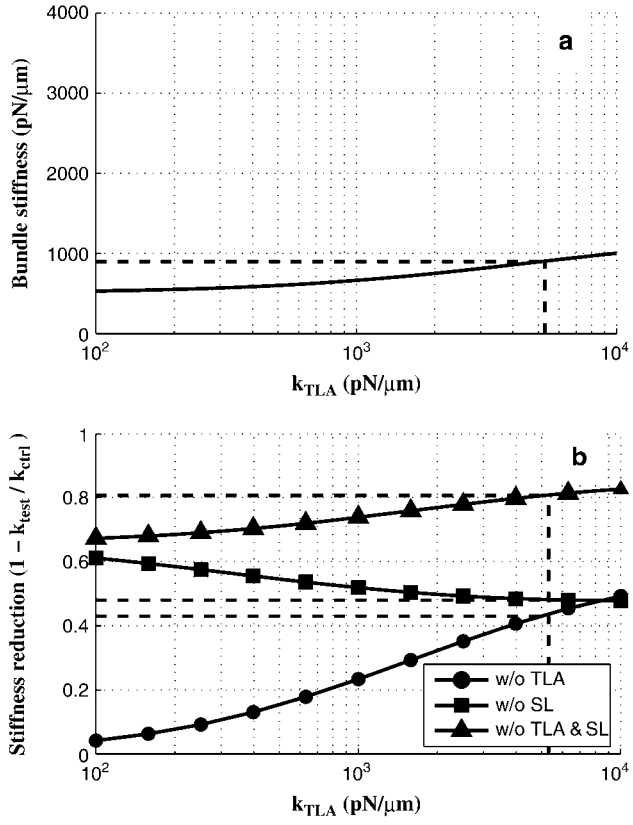

FIGURE 4 Effect of TLA stiffness (k_{TLA}) on the hair bundle stiffness. At $k_{TLA} = 5300$ pN/μm, the bundle stiffness matched the experiment results. (*a*) Bundle stiffness versus tip link stiffness: the bundle stiffness increased from 530 to 1000 pN/μm as k_{TLA} increased from 100 to 10,000 pN/μm. (*b*) Structural contribution of different links: as the tip link stiffness increased, the $\bar{k}_{TL}$ increased and the $\bar{k}_{SL}$ decreased.

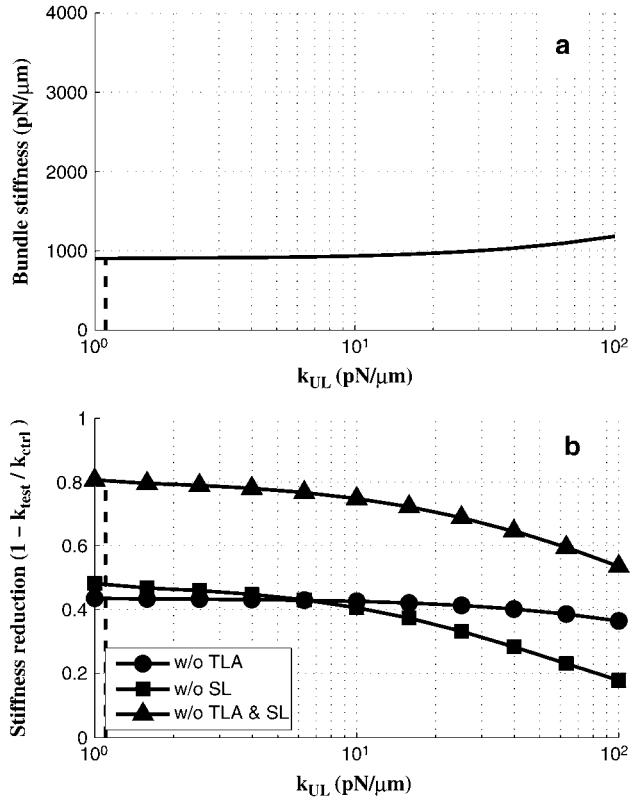

FIGURE 5 Effect of UL stiffness (k_{UL}) on the hair bundle stiffness. The k_{UL} should be close to zero to match the experiment results by Bashtanov et al. (6). (*a*) Bundle stiffness versus UL stiffness: the bundle stiffness increased from 900 to 1180 pN/μm as the UL stiffness increased from 1 to 100 pN/μm. (*b*) Structural contribution of different links: As the k_{UL} increased, the $\bar{k}_{SL}$ decreased, and the $\bar{k}_{TL}$ was not affected much within tested range.

The parametric study of the UL stiffness indicates that the stiffness of ULs should be very small compared to the tip and the SLs (Fig. 5). As the stiffness of the UL approaches zero, the stiffness reduction after tip or SL removal reaches experiment results. Because the ULs connect the adjacent stereocilia horizontally like the SLs, the contribution of the SLs' $\bar{k}_{SL}$ dropped from 0.48 to 0.18 as the stiffness of the UL was increased from 0 to 100 pN/μm. Note that the estimated stiffness of the UL (1 pN/μm) is much smaller than the identified TLA and SL stiffness of 5300 and 750 pN/μm. ULs with such a small stiffness did not contribute to the overall bundle stiffness.

Earlier studies noted that ULs must be stiff to allow the bundle to deform with minimal splay and that adding links of identical structure further down the shaft had little effect (23,26). This work reaches an extended conclusion based upon two differences in the model: this model assumes 1), the lateral links have two discrete structures (ULs and SLs) following two discrete material constitutive laws, and 2), the ULs have a nonlinear force-displacement relationship, which exhibits low stiffness at small displacement but increases to significant stiffness value at larger displacement. This allows tip links to transfer more interciliary force at a small displacement, while protecting the tip links via the ULs at a larger displacement.

The SLs have the second greatest effect on the whole bundle stiffness after the stereocilia rootlet stiffness, represented by the stereocilia Young's modulus (Fig. 6). As the stiffness of SLs was increased from 100 to 10,000 pN/μm, the bundle stiffness increased from 570 to 1890 pN/μm (Fig. 6 *a*). As the stiffness of the SL increases, the stiffness contribution of SLs, $\bar{k}_{SL}$, increases from 0.18 to 0.75, whereas that of the tip links, $\bar{k}_{TL}$, decreases from 0.57 to 0.18.

DISCUSSION

Summary

We have used 3-D FE analyses of a hair bundle from the utricular striola to simulate the experiments of Bashtanov et al. (6). These authors measured the stiffness of striolar hair bundles before and after removal of different link types by BAPTA and/or subtilisin. Our simulations have allowed us to specify some important mechanical properties of stereo-

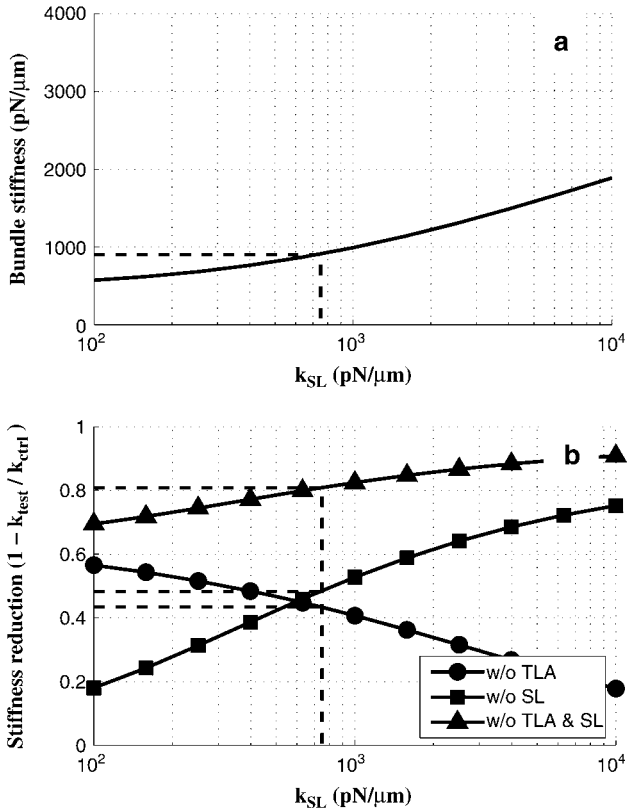

FIGURE 6 Effect of SL stiffness (k_{SL}) on the hair bundle stiffness. At k_{SL} = 750 pN/μm, the bundle stiffness matched the experiment results. (*a*) Bundle stiffness versus SL stiffness: the bundle stiffness increased from 570 to 1890 pN/μm as the k_{SL} increased from 100 to 10,000 pN/μm. (*b*) Structural contribution of different links: as the k_{SL} increased, the $\bar{k}_{SL}$ increased, and the $\bar{k}_{TL}$ decreased.

cilia and of the links that interconnect them. They have also provided insights into the functional role of different interciliary link types. The effects of BAPTA and subtilisin on interciliary links are well documented (for reviews, see Bashtanov et al. (6) and Goodyear et al. (11)), and they were confirmed by those authors using transmission electron microscopy. Accordingly, we assume that the treatment effects we simulated (tip links, SLs, or both removed) accurately reflect the condition of the bundles tested by Bashtanov et al.

Identified mechanical parameters were the Young's modulus of stereocilia at 0.74 GPa, the stiffness of the TLA at 5300 pN/μm, the stiffness of the UL at 1 pN/μm, and the stiffness of the SL at 750 pN/μm. With this set of material properties, the bundle stiffness of the simulated striolar hair bundle from the turtle utricle, 901 pN/μm, matched the experimental stiffness of 900 $\pm$ 500 pN/μm (6). The stiffness reduction after tip link removal was 43.5% in the model, which compares well with the experimental value of 43% $\pm$ 18%. After SL removal, our model results predicted a 48.3% stiffness reduction, again matching the experimental drop of 48% $\pm$ 14%. Finally, after removal of both the tip link and the SL, stiffness drop was 80.8%. This value is less than the 91% estimated in Bashtanov et al. (6). A possible reason for this discrepancy is discussed below (see Why not addition rules in stiffness?).

Although our search for the material properties is systematic, it is not a complete search of the entire solution space. However, Figs. 3–6 show that the model results are well behaved and all but one monotonically change with variation of model inputs. This behavior strongly suggests that no acceptable solution set exists outside our examined parameter space.

Stereocilia

Mechanically, each stereocilium is dominated by bundled actin fibers (46). There are 300–400 actin fibers in the shaft region while the number of fibers reduces as the stereocilium tapers into the root. For striolar hair bundles with heights <10 μm, the stiffness of each stereocilium is governed by the rootlet diameter and the Young's modulus of actin fibers (26). Based on transmission electron micrographs, we determined a stereocilia root diameter of ~40 nm. Using this rootlet diameter, the value of 0.74 GPa was identified. This value is within the range of estimated Young's modulus of 0.1 ~ 10 GPa (47), close to our previous parametric study result of 3 GPa (28) and a recent measurement result of 2 GPa (48). If we overestimated the diameter or the number of actin fibers at the rootlets of the stereocilia, then the identified Young's modulus of stereocilia is underestimated. For example, with a smaller rootlet diameter of 30 nm, the stereocilia Young's modulus would increase to 1.1 GPa, whereas the mechanical properties of extracellular links change less than a few percent.

Tip link assemblies

A tip link is a stranded extracellular filament. This extracellular link is thought to be very stiff so that it can even carry some amount of compressive force (12,14,17). The TLA in our FE model includes not only the extracellular filament, which is thought to be mostly composed of Cdh23 (14), but also any structural elements that are serially connected to it as it spans between the actin cores of adjacent stereocilia. When a stiff spring is serially connected to a compliant spring, the total stiffness of the spring complex is approximated by the compliant element. Therefore, the identified stiffness of TLA in the FE model (5300 pN/μm) will be the approximate stiffness of the compliant structural elements serially connected to the extracellular tip link.

The tip links have long been considered as a gating spring—a compliant elastic link that is serially connected to the transduction channel. Recently, it was suggested that the ankyrin repeats in the transduction channel are the elastic gating spring (12,35,37). Transient receptor potential (TRP) channels are believed to be the transduction channel of the hair cell. Among the TRP family, TRPA1 and NOMPC contain 17 and 29 ankyrin repeats, respectively (15,37). The 17 and 29 ankyrin repeats form an elastic spring and their stiffnesses are estimated as 5000 pN/μm and 900 pN/μm, respectively (15,37). Current evidence supports TRPA1 as a component of the transduction channels in vertebrate hair cells (49).

Our identified stiffness of the TLAs, 5300 pN/μm, represents the stiffness of the gating spring. If the 17 ankyrin repeats in TRPA1 are the gating spring, it requires one ankyrin spring at one end of a tip link or two ankyrin springs at each end of a tip link. (If we assume the ankyrin spring is the most compliant constituent in the TLA and has a stiffness of k_A, two ankyrin springs attached in parallel at one end of the tip link will give the TLA a combined stiffness of $2k_A$. If a pair of ankyrin springs occurs at each end of the tip link, the overall stiffness of the TLA, k_{TLA}, is k_A ($1/k_{TLA} = 1/(2k_A) + 1/(2k_A)$).)

However, considering that all the TRP channels are tetramers (50), the TRPA1 channel may have quadruple ankyrin springs as is illustrated in Howard and Bechstedt (37). If one TRPA1 channel per a tip link has four parallel ankyrin springs, the combined stiffness of these ankyrin springs is 20,000 pN/μm. If there is another TRPA1 channel at the other end of the tip link, the combined stiffness becomes 10,000 pN/μm. These stiffnesses are ~2–4 times our estimated TLA stiffness and as great as 10–20 times the gating spring stiffness estimated by the gating model (19). Two other possibilities exist. One possibility is that the gating spring may be made up of TRP heterotetramers, with some subunits having longer (more compliant) ankyrin repeats. The other possibility is that the ankyrin repeats are not the gating spring and another yet unknown springy protein is the gating spring.

Previously the gating spring stiffness was estimated to be ~1000 pN/μm (19), which is one-fifth of the TLA stiffness in our hair bundle model. This stiffness value is often cited as a measured value. However, the value is estimated from experimental results based on the assumption of a particular mechanical model of the hair bundle. Specifically, the assumption was made that the transduction channels in a hair cell are arranged in parallel (19). In fact, the tip links, especially in the vestibular hair cells, are arranged both in parallel and in series. Furthermore, the estimated stiffness of the gating spring depends on whether one assumes a parallel or parallel-plus-serial arrangement of transduction units (Fig. 7). We believe that our 3-D model more accurately reflects the arrangement of transduction units in living hair bundles and that, consequently, our estimated value of 5300 pN/μm is the more accurate value for the gating spring stiffness.

Upper lateral links

We found that the stiffness of ULs should be <1% of the TLA stiffness to allow the TLA to contribute more than 30% of the whole bundle stiffness (Fig. 5). It also needs to be close to zero to correlate the model stiffness with experiment results. Even though the ULs have negligible stiffness in their resting state, it does not necessarily mean that they have no structural role. Often protein filaments get stiffer as they stretch (47). It is conceivable that the ULs in vestibular hair cells also have nonlinear material properties. Also, the stereocilia in hair bundles missing horizontal connectors often appear fused or splayed (34). From these and our simulation results, we can reason upon the structural role of the ULs.

Two structural roles can be hypothesized. Both are possible if ULs exhibit nonlinear mechanical behavior (Fig. 8). One possible role is to protect the tip links from damage. If the ULs gain stiffness as they are stretched, they could act like a door chain preventing relative motion of stereocilia beyond a certain range and protecting the tip links from hyperextension or rupture. The other possible role is to separate neighboring stereocilia. This may be important because hair bundles with damaged or missing lateral links frequently show fusion of stereocilia (34). We implemented the hypothesized nonlinear characteristics of the ULs (Fig. 8) with our hair bundle computational model to test the feasibility of this idea. Our simulation showed that if the bundle is subjected to a large force in either the positive or negative direction, the stereocilia contact one another at their tips where the lateral links are located (Fig. 9). Thus, ULs may act as separators that prevent stereocilia from fusing together.

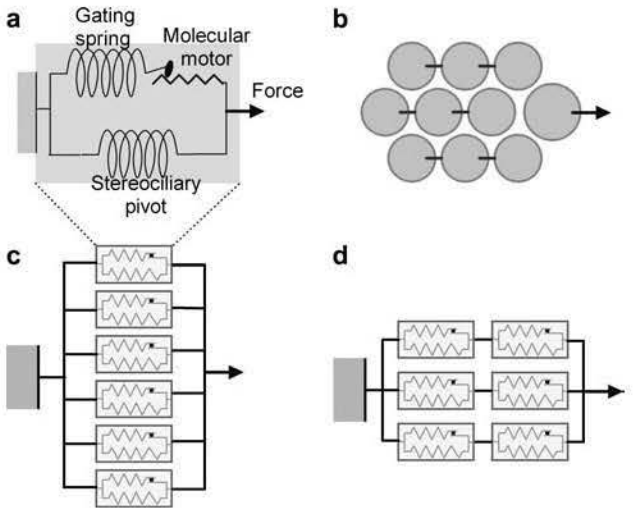

FIGURE 7 Mechanical implication of parallel arrangement assumption. A popular mechanical model of hair bundles represents a transduction unit (two stereocilia linked by a gating spring) as a Maxwell complex (*a*). This transduction unit includes a gating spring, molecular motor (which sometimes includes a damper), and stereociliary pivotal spring. To illustrate the behavior of such transduction units in a 3-D bundle, we examined a hair bundle with nine stereocilia and six transduction units (*b*). In panels *c* and *d*, we show two possible arrangements of the six transduction units (*boxes*). Many studies rely on the parallel arrangement assumption (*c*). According to the parallel arrangement assumption, all transduction units are arranged in parallel. In contrast, our FE model of the hair bundle can be roughly represented by six transduction units arranged like (*d*), i.e., a combined parallel-plus-serial arrangement. If we compare the stiffness of the single channel transduction unit in panels *c* and *d*, the stiffness of a single transduction unit in panel *c* is one-fourth that in panel *d*.

Dilemma with regard to the upper lateral link stiffness

Reported experiments led to a dilemma in our earlier modeling efforts (27,28). Numerous researchers observed bun-

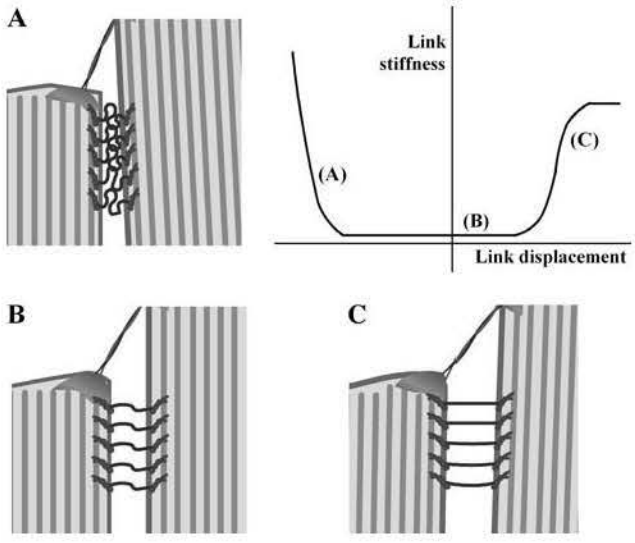

FIGURE 8 Stiffness characteristics of ULs. This study suggests that the stiffness of ULs is nonlinear. In the resting state (*b*), the UL has little stiffness. As it stretches during an excitatory deflection (*c*), it uncoils and becomes stiffer. During an inhibitory deflection (*a*), it behaves like a contact element that prevents the neighboring stereocilia from fusing. This study focused on the initial or resting stiffness when the tip displacement is very small (less than a few nanometers). Within this small displacement range, the ULs are coiled (*b*) and their stiffness is minimal.

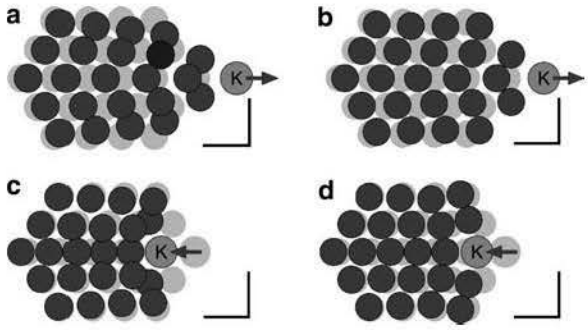

FIGURE 9 ULs can prevent stereocilia from fusing. For this simulation, an ideally symmetric hair bundle was used to avoid possible artifacts of irregular stereocilia spacing. Each plot shows the top view of a deformed hair bundle. Undeformed configurations are shown as background shadows. Top and bottom plots show hair bundles subjected to 400 pN at the tip of kinocilium in the excitatory and 200 pN in the inhibitory directions, respectively. Left plots (*a* and *c*) show the results when allowing contact between stereocilia. Without something to separate them, some stereocilia may fuse together. In the plots at right (*b* and *d*), the ULs are used as a separator or a contact element. The ULs prevented the stereocilia from contacting each other directly.

dles deforming with either no observable or minimal splay (51–53). For all cases the deflection at the tallest end is always seen to be ''transmitted'' to the short end where deflection is also seen. To simulate this transmission requires stiff links to couple stereocilia together. However, tip links only extend along the activation axis of the bundle, so with 3-D vestibular arrays, we also assigned stiff properties to the lateral links (which included both ULs and SLs) to create realistic bundle deflections (28). Further, these stiff lateral links had to be concentrated near the tops of stereocilia to effectively prevent splay. In this way, the mechanical energy needed to deform the shortest stereocilia was transmitted from the tall end of the bundle via the lateral links.

However, stiff lateral links placed near the top of stereocilia resulted in a reduction in tip link tension and the mechanical energy stored there (28). As a result, tip links were mechanically irrelevant to bundle deformation and functioned as passive sensors of motion. This contradicts other experimental observations that mechanical energy must be stored in the tip links (gating springs): tip links were estimated to contribute about half of the hair bundle stiffness (19,44,54,55). Such an observation is not possible without the tip links attached to the gating channels storing significant portions of mechanical energy. The observations of Bashtanov et al. (6) further support the presence of mechanical energy stored in tip links by reporting large differences in stiffness with ablation of tip links.

Our new simulations reconcile these seemingly contradictory mechanical observations. The deformation shape observations (51–53) that were made at larger deflections previously led us to conclude that lateral links must be very stiff and thus to discount the possibility of energy storage in TLAs. The observations showing the mechanical influence of TLAs on bundle stiffness (19,44,54,55) were made at smaller deflections. We posit here that TLAs do not contribute as significantly to the bundle stiffness at larger deflections as at smaller scales. This is possible with nonlinear stiffness of the ULs: by stiffening at large deflections, ULs help prevent splay but they are slack at small deflections, which allows TLAs to transmit mechanical energy efficiently from the tall to the short end of the bundle. In summary, ULs simulated by a linear elastic material response are incapable of matching all experimental results. Further, a close study of the complex morphology and material response of the ULs is vitally important to understanding hair cell dynamics.

Shaft links

Previous hair bundle models have assumed that the ULs and the SLs have the same mechanical properties (23,27,28). Based on that assumption, the SL was shown to have an insignificant role and was not included in the hair bundle mechanical model. But, the experiment results of Bashtanov et al. (6) indicate that the SL contributes as much as 48% of bundle stiffness. According to this finding, we added SLs in the hair bundle FE model with different mechanical properties from ULs. The major structural role of the SLs is apparently to bind the stereocilia together to form a bundle.

Although we computed the stiffness of an SL as 750 pN/μm, this does not mean the absolute stiffness of an actual single SL has that value. Instead, we may say that a group of SLs between a neighboring couple of stereocilia has total stiffness between 750 and 2250 pN/μm (one to three SLs times 750 pN/μm per link). High resolution images of hair bundles show that the links are more densely arranged in real hair bundles than our model (8–10,16). We observed that modeling fewer links doesn't affect the structural response of the hair bundle as long as the total stiffness of the links binding two stereocilia is equivalent. In real hair cells with more SLs between neighboring stereocilia, the stiffness of an individual SL will be smaller than the computed value in this study. In the future, experimental work may determine the actual side link distribution. This would enable direct calculation of the individual link stiffness.

Why not addition rules in stiffness?

Bashtanov and his colleagues estimated the stiffness reduction after removing both the tip links and the SLs as 91%. However, in their experiment the stiffness of bundles treated with both BAPTA and subtilisin could not be measured due to the splitting of the bundle. The estimate of 91% came from the simple summation of the two treatment results: 43% reduction by BAPTA and 48% reduction by subtilisin. Our simulation results suggest that the addition rule does not hold. We saw 81% reduction after removing both types of links, which is 10% less than the estimation based on adding the effects of the two link types. The addition rule holds only

if the hair bundle can be represented by a linear spring model (i.e., adding an SL spring in parallel to the other two springs in Fig. 7 *a*). A simple angular spring and rigid lever model confirmed that $\bar{k}_{SLTL} < \bar{k}_{SL} + \bar{k}_{TL}$. This was just a qualitative test to validate the statement and does not imply that this type of model (angular spring and rigid lever) is a full substitute for our FE model.

Differences between simulation and experiment

There are two potentially important differences between the experiment by Bashtanov et al. and our computational simulations. First, the tested hair cells are from different species. Our model's geometric information was from the turtle utricle, of which geometric characteristics have been studied (31,56). The chosen hair bundle for the simulation is from the striolar region ~20 μm medial to the LPR. Bashtanov's et al. experimental data are from striolar hair cells within 60 μm from the LPR in the chick utricle. The hair cells from different species may have different mechanical/structural characteristics. But, the hair cells used for the simulation and the experiment share two important structural features: the configuration of extracellular links and the height of the bundle. In the simulated hair bundle, the extracellular link configurations were from the chick utricle. Our simulated bundle height is 9.2 μm, and the averaged bundle height of Bashtanov's et al. experiment was ~10 μm (personal communication with G. P. Richardson, University of Sussex, UK, 2005).

Second, the stiffness measurement method is different. In the experiment, the bundle is deflected by the Brownian motion of water molecules. To simulate the Brownian movement is not feasible because it is difficult to quantify the stochastic forces applied by the water molecules. In our simulation a concentrated load is applied at the tip of kinocilium. The different loading conditions may somewhat affect the results. Yet, in the range of experimental resolution, stiffness measurements from observing Brownian motion agree with the stiffness measurement by a concentrated load such as a glass fiber stimulus (57).

CONCLUSIONS

Recent works indicate that there is a rich array of different links in the hair bundle. Our study provides a mechanical interpretation of the effects of those links. Our hair bundle FE model is the first to simulate distinct ULs, SLs, tip links, and KL structures. By matching modeled results to other experiments, we predict the mechanical stiffnesses of different link types. From our predicted TLA mechanical stiffness, we speculate on the gating spring's identity. We also suggest the ULs have nonlinear stiffness values which protect the TLA from rupture or the stereocilia from fusion during large displacements while leaving bundle sensitivity intact for small displacements.

We thank Jingbing Xue and Will Moravec for the confocal images in Fig. 1.

This research was supported by grant DC05063 from the National Institutes of Health.

REFERENCES

1. Cohen, B., and T. Raphan. 2004. The physiology of the vestibuloocular reflex (VOR). *In* The Vestibular System. S. M. Highstein, R. R. Fay, and A. N. Popper, editors. Springer, New York.
2. Keshner, E. A., and H. Cohen. 1989. Current concepts of the vestibular system reviewed: 1. The role of the vestibulospinal system in postural control. *Am. J. Occup. Ther.* 43:320–330.
3. Peterson, B. W., and R. Boyle. 2004. Vestibulocollic reflexes. *In* The Vestibular System. S. M. Highstein, R. R. Fay, and A. N. Popper, editors. Springer, New York.
4. Balaban, C. D., and B. J. Yates. 2004. Vestibuloautonomic interactions: A teleologic perspective. *In* The Vestibular System. S. M. Highstein, R. R. Fay, and A. N. Popper, editors. Springer, New York.
5. Hackney, C. M., and D. N. Furness. 1995. Mechanotransduction in vertebrate hair cells: structure and function of the stereociliary bundle. *Am. J. Physiol.* 268:C1–13.
6. Bashtanov, M. E., R. J. Goodyear, G. P. Richardson, and I. J. Russell. 2004. The mechanical properties of chick (Gallus domesticus) sensory hair bundles: relative contributions of structures sensitive to calcium chelation and subtilisin treatment. *J. Physiol.* 559:287–299.
7. Goodyear, R., and G. Richardson. 1992. Distribution of the 275 kD hair cell antigen and cell surface specialisations on auditory and vestibular hair bundles in the chicken inner ear. *J. Comp. Neurol.* 325: 243–256.
8. Goodyear, R., and G. Richardson. 1994. Differential glycosylation of auditory and vestibular hair bundle proteins revealed by peanut agglutinin. *J. Comp. Neurol.* 345:267–278.
9. Goodyear, R., and G. Richardson. 1999. The ankle-link antigen: an epitope sensitive to calcium chelation associated with the hair-cell surface and the calycal processes of photoreceptors. *J. Neurosci.* 19: 3761–3772.
10. Goodyear, R. J., and G. P. Richardson. 2003. A novel antigen sensitive to calcium chelation that is associated with the tip links and kinocilial links of sensory hair bundles. *J. Neurosci.* 23:4878–4887.
11. Goodyear, R. J., W. Marcotti, C. J. Kros, and G. P. Richardson. 2005. Development and properties of stereociliary link types in hair cells of the mouse cochlea. *J. Comp. Neurol.* 485:75–85.
12. Kachar, B., M. Parakkal, M. Kurc, Y. Zhao, and P. G. Gillespie. 2000. High-resolution structure of hair-cell tip links. *Proc. Natl. Acad. Sci. USA.* 97:13336–13341.
13. Michel, V., R. J. Goodyear, D. Weil, W. Marcotti, I. Perfettini, U. Wolfrum, C. J. Kros, G. P. Richardson, and C. Petit. 2005. Cadherin 23 is a component of the transient lateral links in the developing hair bundles of cochlear sensory cells. *Dev. Biol.* 280:281–294.
14. Sollner, C., G. J. Rauch, J. Siemens, R. Geisler, S. C. Schuster, U. Muller, and T. Nicolson. 2004. Mutations in cadherin 23 affect tip links in zebrafish sensory hair cells. *Nature.* 428:955–959.
15. Sotomayor, M., D. P. Corey, and K. Schulten. 2005. In search of the hair-cell gating spring elastic properties of ankyrin and cadherin repeats. *Structure.* 13:669–682.
16. Tsuprun, V., R. J. Goodyear, and G. P. Richardson. 2004. The structure of tip links and kinocilial links in avian sensory hair bundles. *Biophys. J.* 87:4106–4112.
17. Tsuprun, V., and P. Santi. 2000. Helical structure of hair cell stereocilia tip links in the chinchilla cochlea. *J. Assoc. Res. Otolaryngol.* 1:224–231.
18. Howard, J., and A. J. Hudspeth. 1987. Mechanical relaxation of the hair bundle mediates adaptation in mechanoelectrical transduction by the bullfrog's saccular hair cell. *Proc. Natl. Acad. Sci. USA.* 84:3064–3068.

19. Howard, J., and A. J. Hudspeth. 1988. Compliance of the hair bundle associated with gating of mechanoelectrical transduction channels in the bullfrog's saccular hair cell. *Neuron*. 1:189–199.

20. Stauffer, E. A., J. D. Scarborough, M. Hirono, E. D. Miller, K. Shah, J. A. Mercer, J. R. Holt, and P. G. Gillespie. 2005. Fast adaptation in vestibular hair cells requires Myosin-1c activity. *Neuron*. 47:541–553.

21. Cheung, E. L., and D. P. Corey. 2006. Ca2+ changes the force sensitivity of the hair-cell transduction channel. *Biophys. J.* 90:124–139.

22. Geisler, C. D. 1993. A model of stereociliary tip-link stretches. *Hear. Res.* 65:79–82.

23. Pickles, J. O. 1993. A model for the mechanics of the stereociliar bundle on acousticolateral hair cells. *Hear. Res.* 68:159–172.

24. Cotton, J. R. 1998. Mechanical models of vestibular hair cell bundles. PhD thesis. *In* Engineering Science and Mechanics. Virginia Tech, Blacksburg, VA.

25. Cotton, J. R., and J. W. Grant. 2000. A finite element method for mechanical response of hair cell ciliary bundles. *J. Biomech. Eng.* 122: 44–50.

26. Cotton, J., and W. Grant. 2004. Computational models of hair cell bundle mechanics: I. Single stereocilium. *Hear. Res.* 197:96–104.

27. Cotton, J., and W. Grant. 2004. Computational models of hair cell bundle mechanics: II. Simplified bundle models. *Hear. Res.* 197:105–111.

28. Silber, J., J. Cotton, J. H. Nam, E. H. Peterson, and W. Grant. 2004. Computational models of hair cell bundle mechanics: III. 3-D utricular bundles. *Hear. Res.* 197:112–130.

29. Duncan, R. K., and J. W. Grant. 1997. A finite-element model of inner ear hair bundle micromechanics. *Hear. Res.* 104:15–26.

30. Reddy, J. N. 1993. An Introduction to the Finite Element Method, 2nd ed. (McGraw-Hill series in mechanical engineering). McGraw-Hill, New York.

31. Moravec, W. J., and E. H. Peterson. 2004. Differences between stereocilia numbers on type I and type II vestibular hair cells. *J. Neurophysiol.* 92:3153–3160.

32. Xue, J., and E. H. Peterson. 2006. Hair bundle heights in the utricle: differences between macular locations and hair cell types. *J. Neurophysiol.* 95:171–186.

33. Pickles, J. O., S. D. Comis, and M. P. Osborne. 1984. Cross-links between stereocilia in the guinea pig organ of Corti, and their possible relation to sensory transduction. *Hear. Res.* 15:103–112.

34. Tsuprun, V., P. A. Schachern, S. Cureoglu, and M. Paparella. 2003. Structure of the stereocilia side links and morphology of auditory hair bundle in relation to noise exposure in the chinchilla. *J. Neurocytol.* 32:1117–1128.

35. Corey, D. P., and M. Sotomayor. 2004. Hearing: tightrope act. *Nature*. 428:901–903.

36. Gillespie, P. G., R. A. Dumont, and B. Kachar. 2005. Have we found the tip link, transduction channel, and gating spring of the hair cell? *Curr. Opin. Neurobiol.* 15:389–396.

37. Howard, J., and S. Bechstedt. 2004. Hypothesis: a helix of ankyrin repeats of the NOMPC-TRP ion channel is the gating spring of mechanoreceptors. *Curr. Biol.* 14:R224–R226.

38. Nicolson, T. 2005. Fishing for key players in mechanotransduction. *Trends Neurosci.* 28:140–144.

39. Kikuchi, T., T. Takasaka, A. Tonosaki, and H. Watanabe. 1989. Fine structure of guinea pig vestibular kinocilium. *Acta Otolaryngol.* 108: 26–30.

40. Peterson, E. H., J. R. Cotton, and J. W. Grant. 1996. Structural variation in ciliary bundles of the posterior semicircular canal. Quantitative anatomy and computational analysis. *Ann. N. Y. Acad. Sci.* 781: 85–102.

41. Tilney, L. G., E. H. Egelman, D. J. DeRosier, and J. C. Saunder. 1983. Actin filaments, stereocilia, and hair cells of the bird cochlea. II. Packing of actin filaments in the stereocilia and in the cuticular plate and what happens to the organization when the stereocilia are bent. *J. Cell Biol.* 96:822–834.

42. Tilney, M. S., L. G. Tilney, R. E. Stephens, C. Merte, D. Drenckhahn, D. A. Cotanche, and A. Bretscher. 1989. Preliminary biochemical characterization of the stereocilia and cuticular plate of hair cells of the chick cochlea. *J. Cell Biol.* 109:1711–1723.

43. Hillman, D. E. 1969. New ultrastructural findings regarding a vestibular ciliary apparatus and its possible functional significance. *Brain Res.* 13:407–412.

44. Jaramillo, F., and A. J. Hudspeth. 1993. Displacement-clamp measurement of the forces exerted by gating springs in the hair bundle. *Proc. Natl. Acad. Sci. USA*. 90:1330–1334.

45. Marquis, R. E., and A. J. Hudspeth. 1997. Effects of extracellular Ca2+ concentration on hair-bundle stiffness and gating-spring integrity in hair cells. *Proc. Natl. Acad. Sci. USA*. 94:11923–11928.

46. Tilney, L. G., D. J. Derosier, and M. J. Mulroy. 1980. The organization of actin filaments in the stereocilia of cochlear hair cells. *J. Cell Biol.* 86:244–259.

47. Howard, J. 2000. Mechanics of Motor Proteins and the Cytoskeleton. Sinauer Associates, Sunderland, MA.

48. Shin, J. H., L. Mahadevan, P. T. So, and P. Matsudaira. 2004. Bending stiffness of a crystalline actin bundle. *J. Mol. Biol.* 337:255–261.

49. Corey, D. P., J. Garcia-Anoveros, J. R. Holt, K. Y. Kwan, S. Y. Lin, M. A. Vollrath, A. Amalfitano, E. L. Cheung, B. H. Derfler, A. Duggan, G. S. Geleoc, P. A. Gray, M. P. Hoffman, H. L. Rehm, D. Tamasauskas, and D. S. Zhang. 2004. TRPA1 is a candidate for the mechanosensitive transduction channel of vertebrate hair cells. *Nature*. 432:723–730.

50. Clapham, D. E. 2003. TRP channels as cellular sensors. *Nature*. 426: 517–524.

51. Flock, A., B. Flock, and E. Murray. 1977. Studies on the sensory hairs of receptor cells in the inner ear. *Acta Otolaryngol.* 83:85–91.

52. Hudspeth, A. J. 1983. The hair cells of the inner ear. *Sci. Am.* 248: 54–64.

53. Corey, D. P., P. L. Huang, and J. A. Assad. 1989. Hair cell stereocilia bend at the bases and touch at their tips. *Soc. Neurosci.* 15:208. (Abstr.).

54. Geleoc, G. S., G. W. Lennan, G. P. Richardson, and C. J. Kros. 1997. A quantitative comparison of mechanoelectrical transduction in vestibular and auditory hair cells of neonatal mice. *Proc. R. Soc. Lond. B*. 264:611–621.

55. Ricci, A. J., A. C. Crawford, and R. Fettiplace. 2002. Mechanisms of active hair bundle motion in auditory hair cells. *J. Neurosci.* 22:44–52.

56. Xue, J., and E. H. Peterson. 2004. Organization of the utricular striola in Trachemys scripta: bundle heights. *ARO midwinter meeting*.

57. Denk, W., W. W. Webb, and A. J. Hudspeth. 1989. Mechanical properties of sensory hair bundles are reflected in their Brownian motion measured with a laser differential interferometer. *Proc. Natl. Acad. Sci. USA*. 86:5371–5375.